Simulation studies for the detection of changes in broadband albedo and shortwave nadir reflectance spectra under a climate change scenario

Daniel R. Feldman,[1] Chris A. Algieri,[2] William D. Collins,[1,3] Yolanda L. Roberts,[4,5] and Peter A. Pilewskie[4,5]

Climate forcing by greenhouse gases and aerosols and climate feedbacks from snow, sea-ice, and clouds all significantly impact the future evolution of the climate system's shortwave energy budget. We examine prospects for tracking changes in these forcings and feedbacks using top-of-atmosphere measurements of shortwave reflected radiation. We quantify the extent to which spectral measurements may reduce the time required to detect changes in the climate the climate system with high statistical confidence relative to conventional broadband measurements. We have developed an Observing System Simulation Experiment (OSSE) based on the Community Climate System Model 3.0 for the NASA CLARREO mission and have analyzed forced and unforced simulations of the 21st Century from the Intergovernmental Panel on Climate Change assessments. We find that changes in the simulated nadir spectral reflectance measurements in the visible window and between near-infrared water-vapor overtone channels under clear-sky conditions are detectible faster than the corresponding changes in broadband albedo, with many trends detectible within a five-year satellite mission lifetime. Under all-sky conditions, the superposition of unforced cloud variability on the secular climate trends lengthens the times required for climate-change detection in both the spectral and broadband data. However, migration of the ITCZ and stratus regions can be detected after 16–18 years of observation while broadband albedo measurements require 33–61 years of observation. We find that measurement uncertainty and instrument drift significantly lengthen detection times for broadband albedo and spectral reflectances in window channels but do not have the same effect for spectral measurements in water vapor bands.

1. Introduction

The Earth's albedo governs the amount of solar radiation absorbed by the climate system and results from complex interactions among many radiative processes in the atmosphere and at the planetary surface. Spatial and temporal variations in clouds, vegetation, sea-ice, snow, and other components of the climate system can easily lead to localized fluctuations in the top-of-atmosphere albedo of 20% to 80%. The fact that the global annual-mean planetary albedo does not exhibit large interannual changes despite the large variability in these contributing components suggests that there could be negative feedbacks that dampen fluctuations in it [Schwartz et al., 2010]. In theory, globally and annually averaged albedo deviations of 1% in absolute units, or equivalently around 3 W/m^2, would either completely cancel or significantly augment historical anthropogenic climate forcings depending on the sign of the albedo change [Intergovernmental Panel on Climate Change (IPCC), 2007, chapter 2]. Thus, there is a compelling societal need to determine the climate conditions under which albedo is and is not stable, and identification of these conditions requires an understanding of the forcings and feedbacks that maintain or cause changes in this quantity.

Ideally, unequivocal measurements of albedo and correlative data on the feedback processes that control albedo would be used to inform climate model simulations. This would help ensure that the scientific community would have robust prediction capabilities for the changes in the planetary albedo and outgoing longwave radiation that would result

[1]Earth Sciences Division, Lawrence Berkeley National Laboratory, Berkeley, California, USA.
[2]Climate Sciences Department, Lawrence Berkeley National Laboratory, Berkeley, California, USA.
[3]Department of Earth and Planetary Science, University of California, Berkeley, California, USA.
[4]Department of Atmospheric and Oceanic Science, University of Colorado at Boulder, Boulder, Colorado, USA.
[5]Laboratory for Atmospheric and Space Physics, University of Colorado at Boulder, Boulder, Colorado, USA.

from a given set of climate forcings. Having a comprehensive and internally consistent data set of top-of-atmosphere albedo measurements is a necessary condition toward reaching that goal. Necessary and sufficient conditions require a combination of very accurate and stable albedo time series to detect the trends combined with the coincident measurements needed to attribute these trends to systematic changes in one or more components of the climate system that affect albedo with a high degree of confidence. Unfortunately, observational determination of the Earth's albedo is very challenging for several reasons including: (1) temporal and spatial resolution of the measurements, (2) instrument calibration drift, (3) conversion of measured radiance to hemispheric flux, and (4) the stringent requirement of measurement signal-to-noise ratio.

[4] Extensive work has been performed as part of the ERBE [*Barkstrom and Smith*, 1986] and CERES [*Wielicki et al.*, 1996] missions to provide climate-quality albedo data derived from raw radiance measurements, and these missions have determined patterns of albedo at spatial and temporal scales of one month and $1° \times 1°$, respectively, with a bias error of 0.2 W/m^2 and an RMS error of 1.0 W/m^2 after some ad hoc adjustment and corrections [*Loeb et al.*, 2009].

[5] Recently, there has been considerable debate surrounding the long-term stability of the Earth's albedo with significant implications for the near-term trajectory of climate change. The issue has arisen because of apparent inconsistencies between direct and indirect observational records of the Earth's reflected solar radiation. While *Pallé et al.* [2004] looked at Earthshine data and found evidence of global dimming with a steady decrease in the Earth's reflectance from 1984 to 2000 followed by an increase between 2001 and 2003, *Wielicki et al.* [2005] found no trend in planetary albedo from an analysis of CERES data coupled with other correlative satellite records from the MODerate Resolution Imaging Spectrometer (MODIS) [*Justice et al.*, 1998] and Jason/TOPEX [*Ducet et al.*, 2000]. More recently, *Pallé et al.* [2009] performed a reanalysis of the Earthshine data and a recalibration of the CERES products and, based upon this new analysis, concluded that there is no trend in planetary albedo. The debate surrounding trend estimation from long-term satellite-based records is not new, but it is of critical scientific importance to determine whether there is a small secular trend in a long-term albedo data set. This task is greatly complicated by the nearly inevitable drift in instrument calibration after launch [e.g., *Hurrell and Trenberth*, 1998] combined with the deleterious effects of near-Earth environment on instrument performance [e.g., *Tashima and Hartmann*, 1999].

[6] To address these issues, the National Research Council's Space Studies Board has recommended launching a new satellite mission to collect absolutely calibrated measurements of the Earth's solar reflectance and infrared emission measured at nadir for robust detection and quantification of trends in the climate system [*Space Studies Board*, 2007]. The mission is called the CLimate Absolute Radiance and Refractivity Observatory (CLARREO) and is designed to measure nadir shortwave reflectances, infrared radiances, and GPS radio-occultation profiles from a satellite platform. The calibration standard for these measurements calls for rigorous traceability, via multiple and independent metrological pathways, to fundamental standards of length, mass, time, temperature, and energy [*Anderson et al.*, 2004]. The exacting nature of the calibration standards of the CLARREO measurements is critical both for determining whether the measurements are stable over the lifetime of the instrument and for comparing such measurements against future and previous data. If successful, the CLARREO mission will be free of the challenges stemming from uncertain calibration and instrumental artifacts that complicate current efforts to determine long-term trends in the Earth's radiation balance.

[7] However, it is important to note that CLARREO is not intended to serve as a new type of radiation-budget mission since it lacks the spatial coverage and range of viewing angles required to adequately sample the eight-dimensional phase space of the reflected solar radiation [*Wielicki et al.*, 1995]. This means that the CLARREO measurements will be interpreted in their original form without the uncertainties introduced in missions such as CERES by the complex empirical algorithms to convert filtered radiances into unfiltered hemispherical fluxes and to interpolate these fluxes in space and time to estimate the whole Earth's radiation field [*Young et al.*, 1998] Nor is it intended as a new type of process-oriented mission by extending extant channel-based spectrometers (e.g., MODIS) into the hyperspectral domain for the purpose of retrieving geophysical parameters from the radiance data. In the analysis that follows, we will analyze the simulated CLARREO radiance data its original radiometric form modified only by spatial and temporal averaging and by conversion from radiances to nadir reflectances through division by the coincidentally measured incident solar spectrum.

[8] Although this study has been undertaken to quantify the change in detection times and confidence levels for climate-change signals afforded by CLARREO, the Observing System Simulation Experiment (OSSE) framework and its results are applicable to a wide range of hypothetical space-based hyperspectral measurements of the solar and infrared spectrum calibrated in a rigorously traceable manner against absolute standards. The analysis that follows targets the CLARREO satellite and its suite of measurements for the sake of concreteness, but CLARREO should be considered as an archetype for a series of missions to detect and attribute the radiative signals of climate change. Extensive work has already elucidated the utility of the spectrally resolved IR measurements both in terms of the suite of existing instrumentation and in terms of the measurements' impact on an understanding of the climate system under climate change scenarios [*Haskins et al.*, 1997; *Goody et al.*, 1998; *Harries et al.*, 2001; *Huang and Ramaswamy*, 2009; *Huang et al.*, 2010]. The distinguishing and novel feature of the present work is the extension to visible and near-infrared wavelengths using the framework developed by *Feldman et al.* [2011].

[9] The shortwave instrument is designed to measure the nadir reflectance of solar radiation from Earth to space between 320 to 2300 nm at 8 nm Full-Width Half-Maximum spectral resolution. The limits on the wavelength range have been chosen to maximize the spectral coverage while simultaneously ensuring that the nadir reflectances attain a 2σ-accuracy of 0.3% over the entire spectral range. While individual footprints are 0.5×0.5 km for solar/lunar calibration and for cloud masking of clear/cloudy spectra, the

absolute accuracy for CLARREO is only required for large space/time averaged data. The range extends from the near-UV to the middle of the near-IR and encompasses over 99% of the energy incident in the top of atmosphere (TOA) insolation. This instrument is distinguished relative to most previous space-borne visible and near-infrared imagers by the continuity of its spectral coverage. Existing satellite instruments used for Earth observing with this characteristic are limited in number and include the Hyperion [*Pearlman et al.*, 2003] sensor onboard NASA's EO-1 satellite [*Ungar et al.*, 2003] and the SCIAMACHY sensor onboard ESA's Envisat platform [*Bovensmann et al.*, 1999]. The other distinguishing characteristic is a set of on-orbit requirements for accuracy, stability, and calibration that are unprecedented relative to existing measurements [*Kopp et al.*, 2009]. The spatial resolution of nadir-pointing pixels is 0.5×0.5 km and is sufficient to differentiate between cloudy and clear scenes with an accuracy of 2–3% [*Wielicki and Parker*, 1992].

[10] Prior to the deployment of a new measurement system, it is important to determine its utility relative to current systems both in terms of the specific objectives of the proposed mission and its context within observational Earth science. In the case of CLARREO and other comparable missions, the central issue is the scientific value added from spectrally resolved nadir reflectance data relative to the combination of broadband Earth radiation data and narrowband retrievals of the geophysical parameters that govern the radiation field provided by current instrument suites such as the NASA A-train.

[11] Therefore, this paper seeks to address the utility of making spectrally resolved nadir reflectance measurements relative to broadband albedo measurements through an Observing System Simulation Experiment (OSSE). One of the purposes of the OSSE is to determine the reductions (if any) in the observing time required to detect climate change with high confidence that follow from spectrally resolved nadir reflectance measurements spanning 99% of the solar insolation. While measurements of spectral albedo have not been proposed and are therefore purely hypothetical, climate-change signals in broadband and spectral albedos would differ primarily due to the addition of spectral resolution, and climate-change signals in spectral albedos and nadir reflectances would differ primarily due to the differences in angular sampling. Therefore we analyze simulations of broadband albedo, spectral albedo, and nadir spectral reflectance in order to be able to separate the effects of solid-angle integration from the effects of spectral resolution and continuity on detection times. In the following analysis, the utility of shortwave spectral measurements is demonstrated by simulating the existing broadband and proposed hyperspectral measurements under projected climate-change conditions. The simulations are used to gauge the impact of the nadir hyperspectral reflectances on the time required to detect secular trends in the shortwave energy budget. As we show below, the nadir reflectance spectra are useful for detecting anthropogenic changes in the shortwave energy budget more rapidly than is possible with current measurements because of the sensitivity of the spectra to changes in the absorption and reflection of sunlight by the Earth's surface and atmosphere.

[12] To address these questions, this paper is organized as follows: first, in the methodology section we describe the OSSE framework and its output that form the basis of this work. Next, we discuss the methods used and assumptions made in the statistical analysis of the OSSE data. The OSSE is applied to simulations of the 21st century from the IPCC Fourth Assessment Report (AR4) [*IPCC*, 2007] based on the Special Report on Emissions Scenarios (SRES) A2 emissions scenario [*IPCC*, 2000]. The OSSE outputs are analyzed to estimate the time required to detect changes in shortwave broadband or spectral albedo and nadir reflectance assuming a complete data record for the entire 21st century. The detection times are affected by the presence of natural variability, and we describe our characterization of that variability using OSSE simulations based upon the IPCC AR4 constant-concentrations scenario [*Meehl et al.*, 2005]. Our analysis is focused on determining the amount of time that would be required to detect changes in these quantities unambiguously from a partial data record, where statistics are compiled only from the partial record. In practice researchers will want to determine the minimum duration of observations required to make definitive statements about change detection. Finally, we explore how instrument drift and total measurement uncertainty (including orbital sampling noise and reference intercalibration error) lengthen the time required to detect changes in broadband albedo and nadir spectral reflectance, and we discuss the findings in terms of how they may serve as a guide for future research in terms of remote sensing of the shortwave energy budget.

2. Methodology

[13] Simulations of a notional shortwave reflectance instrument with our OSSE have been performed for the 21st Century for two different emissions scenarios. The inputs to the OSSE consist of output from a simulation from the Community Climate System Model [*Collins et al.*, 2006a; *Meehl et al.*, 2006]. The simulation is forced with historical emission estimates of greenhouse gases and aerosols until the year 2000, after which it is forced by the SRES A2 emissions scenario between 2000 and 2100 [*IPCC*, 2000] (hereafter referred to as the "experiment"). The state information required for radiative calculations in the OSSE are available in the monthly mean output files from the CCSM3 integrations. The fact that the state information has been time averaged means the OSSE cannot detect temporal variability on shorter than seasonal timescales, but this filtering in time still permits the OSSE to serve our primary objective to detect long-term trends.

[14] As detailed by *Feldman et al.* [2011], radiative transfer calculations of broadband clear-sky and all-sky fluxes have been performed with the CCSM3 radiation code [*Collins et al.*, 2006b] and with MODTRAN™ version 5.3.0.0 [*Berk et al.*, 1999]. The fluxes from these calculations have been subjected to extensive validation so that the calculated flux values from the CCSM radiation code generally agree to within 1% of the calculations from MODTRAN. Spectrally resolved clear-sky and all-sky flux and radiance quantities have also been computed from MODTRAN and are completely consistent with the collocated and coincident broadband fluxes. Moreover, the time series analysis, as described below, of broadband signals is performed both for results produced by the CCSM3 radiation code and the corresponding MODTRAN code, and the findings generally

agree to within 5%. All data have been calculated based on a nominal sun-synchronous low-earth (700-km altitude) orbit with a 1:30 P.M. local equator crossing time on the ascending node of the orbit. The data are recorded both at the native band-model spectral resolution of 15 cm^{-1} and at the 8 nm resolution planned for the CLARREO instrument by convolving the 15 cm^{-1} output fields with a Gaussian spectral response function employing a 8 nm Full-Width Half-Maximum spread.

[15] Both simulations report the data on the same grid used for the atmospheric component of the CCSM3 simulations. Meridians and parallels at T85 spatial resolution delineate the rectilinear grid where T85 refers to a triangular truncation of the spectral wave number space of the modeled dynamic and thermodynamic fields at 85 wave numbers. Meridians are separated by 1.41°, and there are 128 parallels corresponding to a 128-point Gaussian quadrature over 180° from pole to pole.

[16] In this work, broadband and spectral albedos are denoted by the symbols α and α_λ, respectively, and are calculated as the ratio of upwelling TOA flux to downwelling TOA solar flux, and nadir reflectances are unitless quantities calculated as follows:

$$R_\lambda = \frac{\pi I_\lambda}{F_\lambda^-} \tag{1}$$

where R_λ is the top-of-atmosphere (TOA) nadir reflectance with a viewing zenith angle of 0°, I_λ is the TOA upwelling radiance and is multiplied by π steradians, and F_λ^- is the downwelling TOA flux with all quantities reported at an individual wavelength band centered at λ. Annually and zonally averaged time series data points of albedos and nadir reflectances are produced first by taking arithmetic means of fluxes and radiances over the season of interest and dividing by the arithmetic mean of the TOA incoming solar flux.

[17] At each latitude band, a time series is analyzed according to the methods presented by *Weatherhead et al.* [1998]. Accordingly, we assume that data from the OSSE described above can be represented by the following ansatz:

$$Y_t = \mu + \omega X_t + N_t \tag{2}$$

where Y_t is the zonally and seasonally averaged value of the quantity of interest (either broadband albedo, spectral albedo, or nadir spectral reflectance) at time t, μ is its detrended time-mean value, ω is its secular trend, and X_t is the linear trend function and is identical to the temporal coordinate in the analysis that follows. N_t is the noise term and represents the part of the time series that is not explained by the decomposition of the time series into a sum of a detrended mean and a secular trend. We assume that N_t has a time-mean value of zero and can be described using a low-order stochastic process. Consistent with equation (2), subsequent statistical analysis of the time series requires estimates of the trend in the quantity of interest and of the magnitude and temporal covariance of the noise derived from a detrended and zero-centered version of the time series.

[18] For the former requirement, secular trends are estimated using least squares linear regression of all or part of the time series. For the latter requirement, we start with a simple model and assert that the noise can be described as a first-order autoregressive, or AR(1), process. The form of this process is

$$N_t = \phi N_{t-1} + \varepsilon_t \tag{3}$$

where ϕ is the autocorrelation given by:

$$\phi = Corr(N_t, N_{t-1}) \tag{4}$$

and ε_t is related to the variance of the white-noise component of the time series by:

$$\sigma_\varepsilon^2 = \mathrm{var}(\varepsilon_t). \tag{5}$$

[19] The AR(1) process has been adopted for the purposes of this initial analysis as one of the simpler noise processes that can account for persistence in the fluctuating components of the OSSE fields. However, we recognize that many descriptions of the noise process are possible including higher-order autoregressive processes [*von Storch and Zwiers*, 1999, chapter 10]. The noise process parameters can be derived from the detrended OSSE experiment run or from the OSSE control run, but for this analysis, we have used the latter data set since it has time-invariant boundary conditions suitable for characterizing unforced internal variability.

[20] From the AR(1) model, *Weatherhead et al.* [1998] has determined that the time required to detect a secular change in the zonally and seasonally averaged time series with 95% confidence is:

$$n_U^* \approx \left[\frac{3.96\,\sigma_e}{|\omega_o|(1-\phi)}\right]^{2/3} \tag{6}$$

where n_U^* is the detection time from unforced variability derived from a complete time series and ω_o is underlying secular trend in the data. The multiplier of 3.96 on the white-noise term σ_e is indicative of the uncertainty associated with performing a least squares trend estimation to the 95% confidence level (note that *Weatherhead et al.* [1998] list a factor is 3.3 for the 90% confidence level, but different confidence levels can be obtained from trend uncertainty analysis based on standard normal tables as shown by *Tiao et al.* [1990]). As expected, the time to detection increases with decreasing signal-to-noise ratios ω_0/σ_e. It also increases with increasing positive correlation in the noise process as $\phi \rightarrow 1$ which implies temporally correlated noise and results in highly persistent fluctuations away the long-term mean μ that are difficult to distinguish from the underlying trend. Given that the parameters to calculate detection time will be better estimated with a time series of longer length, *Weatherhead et al.* [1998] showed that the 95% confidence interval for the time required to detect a secular trend in a data record given a finite record length and imperfect estimation of noise parameters, can be expressed as:

$$\left(\hat{n}_u^* e^{-B}, \hat{n}_u^* e^{B}\right) \tag{7}$$

[21] Here $\hat{n}_U^*$ is the estimate of the detection time from equation (6) using the finite-record parameter estimates $\hat{\phi}$, $\hat{\omega}$,

and $\hat{\sigma}_e$ corresponding to ϕ, ω_o, and σ_e, respectively. B, which describes the uncertainty in parameter estimation from a finite record, is given by:

$$B = \frac{4}{3\sqrt{M}} \sqrt{\frac{1+\hat{\phi}}{1-\hat{\phi}}} \tag{8}$$

where M is the record length. Note that equation (7) assumes that the estimates of ϕ, σ_e and ω_o are unbiased and leading to an unbiased estimation of the confidence intervals. The lower and upper bounds set the minimum and maximum record length required to detect statistically significant trends in the quantity of interest to within the desired degree of confidence. As a corollary to this, we can use equation (7) to provide an estimate of the length of measurement record one would need to make definitive statements about whether change is occurring in the measurements given that the noise process parameters may be a function of the record length.

[22] One of the main challenges in the detection and attribution of future climate change is that researchers only have the historical portion of the time series from which to make an assessment about prospective detection times. Because the analysis of time series to search for emergent climate change cannot be purely retrospective, this paper presents a metric for time-signal analysis in which we derive the length of a time series required for definitive detection to within the desired degree of confidence. This metric establishes an upper bound on detection time for secular trends emerging from an observational record that is growing in length.

[23] With a 100-year time series derived from the OSSE calculation, we can analyze the entire record to determine the point where statistically significant change occurred. Also, we can analyze a measurement time series of a shorter length using equation (7) and inquire if an analysis of a subset of the entire record yields the upper bound in detection time that is shorter than the length of the subset. Where it does, it can be declared with statistical confidence that, despite having an incomplete data set, a secular change has occurred in the time series. This formulation is relevant to the goals of early detection of climate change and can be expressed with the following:

$$\hat{n}_U = \min\left(e^B \left[\frac{3.96\,\hat{\sigma}_e(t)}{|\hat{\omega}_o(t)|(1-\hat{\phi}(t))} \right]^{2/3} < t \right) \tag{9}$$

where $\hat{n}_U$ is a robust estimate of the detection time derived from an incomplete time series and $\hat{\sigma}_e(t)$, $\hat{\omega}_o(t)$, and $\hat{\phi}(t)$ refer to the white noise, secular trend, and autocorrelation, respectively, that are derived from a subset of the time series starting at the first element and ending at element t. In order to rule out change detection derived from a very small number of data points, equation (9) is evaluated with record with a minimum length of 5 years.

[24] Whereas the *Weatherhead et al.* [1998] method provides a straightforward approach to estimating change detection time where measurement error is not a major factor, a more general method detailed by *Leroy et al.* [2008a] provides estimates for change detection time where measurement error cannot be neglected. Briefly, *Leroy et al.* [2008a] generalize the findings of *Weatherhead et al.* [1998] and show that the detection time n^*_{U+I} in the presence of natural variability for an imperfect measurement can be described as the following:

$$\hat{n}_{U+I} = \min\left(e^B \left[\frac{3.96\,\hat{\sigma}_e(t)}{|\hat{\omega}_o(t)|(1-\hat{\phi}(t))} \right]^{2/3} \left(1+f^2\right)^{1/3} < t \right) \tag{10}$$

where f is the ratio of the total measurement uncertainty multiplied by its autocorrelation time scale to natural variability multiplied by its autocorrelation time scale. For the subsequent analysis, we assume that autocorrelation time scale for the measurement imperfection is 5 years, corresponding to absolute calibration drift over a typical mission lifetime and justified by *Leroy et al.* [2008a]. For natural variability, we assume the autocorrelation time scale is one year, which allows for the description of the autoregressive noise process. It should be noted here that equation (9) and equation (10) have indeterminate results under conditions where the change detection time for the time series or any given subset of that record is greater than the length of the time series or length of the subset, respectively. Given the threshold formulation in both of these equations, conditions may be encountered where a given time series may produce a determinate change detection time while another time series with slightly different noise parameters, secular trends or measurement uncertainty may have an indeterminate change detection time.

[25] These methods can be used to analyze the OSSE data to address the key science question of how long it will take to detect climate change signals in the presence of both instrumental noise and natural/unforced variability.

3. Results

[26] The OSSE data from the A2 experiment contain signals of major forcing agents including long-lived greenhouse gases (LLGHGs) and anthropogenic aerosols as prescribed by the emissions scenario. The LLGHGs increase steadily throughout the 21st Century while the aerosols increase between 2000 and 2050 and then decrease to pre-industrial levels by 2100. Figures 1a–1f show the projected zonally and annually averaged response of the climate model to the A2 forcing scenario relative to the zonal averages over the decade from 2000 to 2010. Differences in aerosol optical depth, total column water vapor, low and high clouds, and snow-fraction and sea-ice areal extent characterize the forcing and response of the system. Changes in the aerosol optical depth are primarily due to changes in the concentrations of sulfate and carbonaceous aerosols [*Collins et al.*, 2004] prescribed by the A2 emissions scenario and additional assumptions governing the hygroscopicity of the carbonaceous species [*Meehl et al.*, 2006]. The response of the water vapor column is largely governed by the thermodynamics associated with increased surface temperatures. The long-term trends in low, high, and total cloud cover, snow fraction and sea-ice areal extent are all the results of feedback mechanisms within CCSM3 [*Kiehl et al.*, 2006]. The southward movement of the Intertropical Convergence Zone (ITCZ) can be seen in the equatorial time series of low and total cloud amount in Figures 1c and 1d respectively while

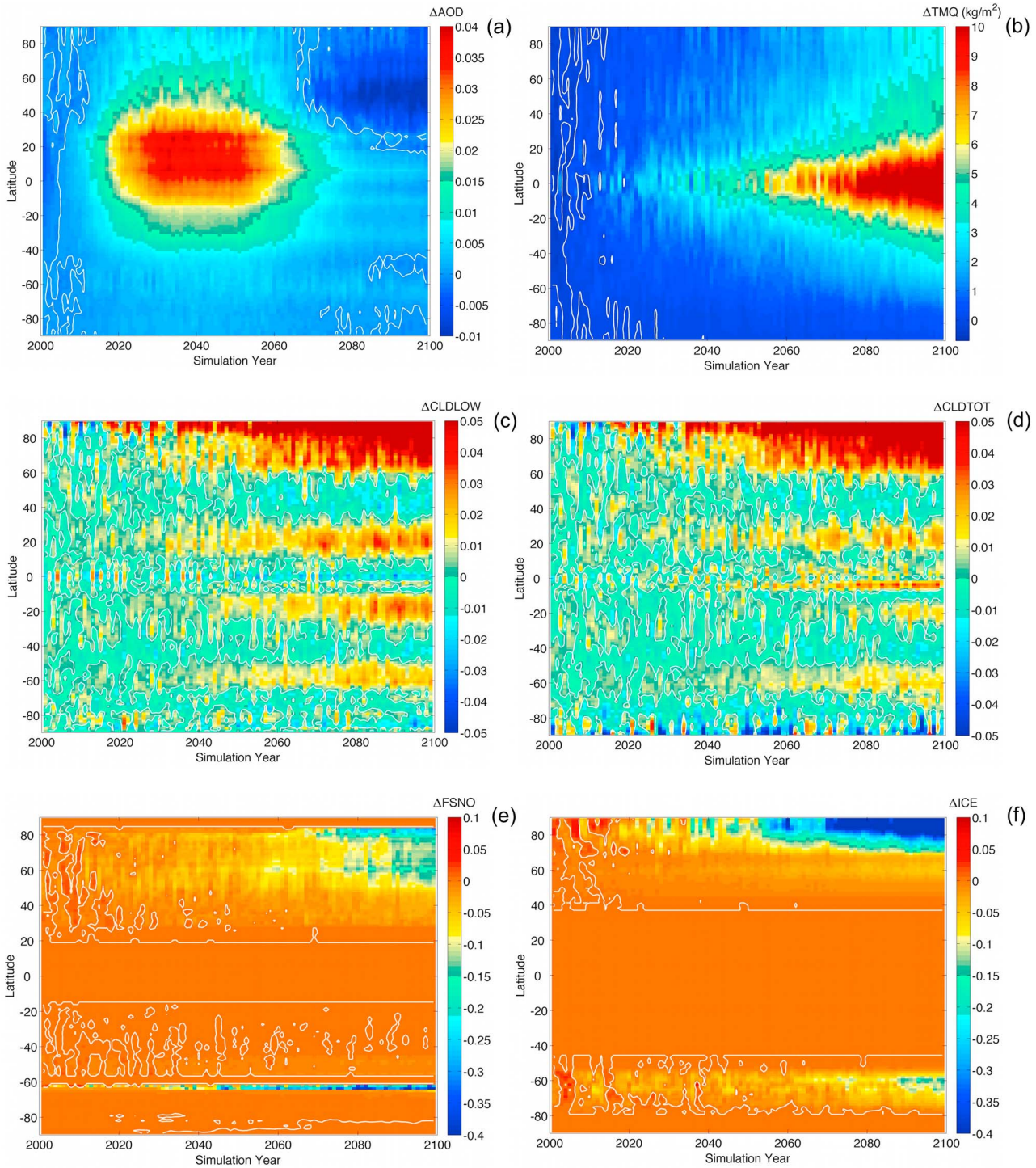

Figure 1. Changes in the zonal mean values of (a) aerosol optical depth, (b) total column water vapor, (c) low cloud fraction, (d) total cloud fraction, (e) snow fraction and (f) sea ice fractional area from the A2 simulation of the 21st Century computed by differencing these fields at a given time step with those same zonally averaged fields also temporally averaged over the period 2000–2009. For all plots, white contours denote zero difference line.

a strengthening of the stratus cover can be seen in the increase in low cloud amount around ±20° in Figure 1c. Meanwhile, poleward movement of the midlatitude storm tracks is also manifested by decreasing cloud cover at ±40° and increasing cloud amount at ±60°. Zonally averaged fractional snow coverage decreases at high- and midlatitudes as governed by feedback processes built into the Community Land Model [*Dickinson et al.*, 2006], while similar decreases in the sea-ice area extent are governed by the Community Sea Ice Model [*Briegleb et al.*, 2004] that is integrated into

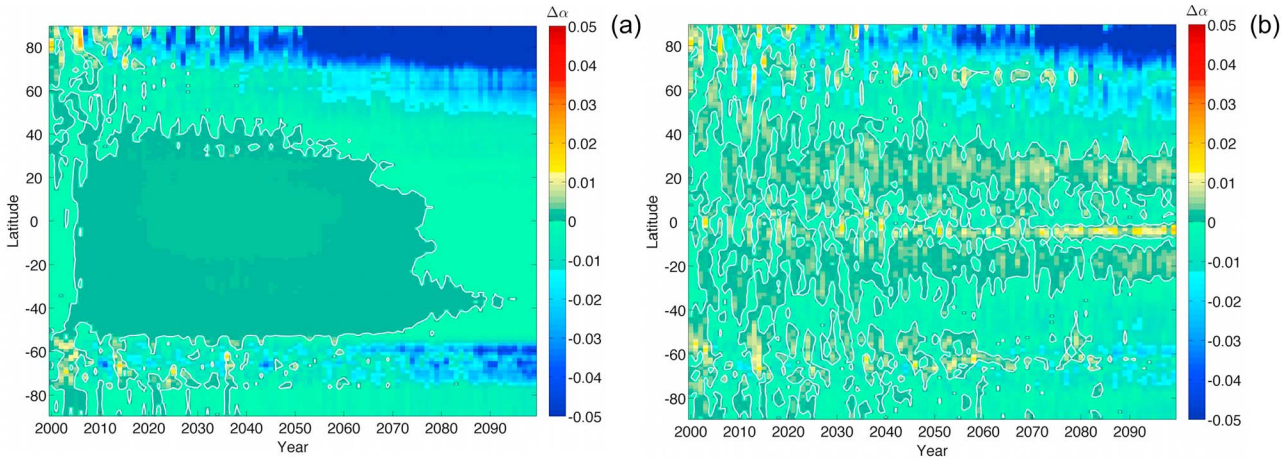

Figure 2. Zonally and annually averaged time series of the changes in shortwave broadband albedo between each year of the simulation and the time-mean zonally averaged albedo during 2000–2009 for (a) clear-sky conditions and (b) all-sky conditions. For both plots, white contours denote zero difference line.

CCSM3. All of these components of the climate system affect broadband albedos and nadir spectral reflectances, and it is clear from these plots that the time series of the quantities displayed have a secular trend superimposed on a significant amount of natural/unforced variability.

[27] The quantities plotted in Figures 1a–1f are manifested in the annually and zonally averaged albedo plots shown in Figures 2a and 2b. These latter figures show the time series of changes in clear- and all-sky broadband albedos between each year of the 21-century simulations and the beginning of the simulation record spanning 2000 to 2010. It is apparent that in the clear-sky time series, the broadband albedo increases in lower latitudes throughout the first half of the 21st Century and returns to present-day conditions by the end of the Century. This combination of an initial brightening transitioning to subsequent darkening at mid-century can largely be attributed to the time series of anthropogenic aerosol loading prescribed in the A2 emissions scenario. At higher southern latitudes, there are fluctuations in broadband albedo that are directly tied to the sea-ice areal extent feedback while at higher northern latitudes, snow fraction and sea-ice extent feedbacks also dramatically reduce the broadband albedos after 2050. Some of these forcing and feedback signals are obscured by the presence of clouds as evidenced by the lower magnitudes of these signals in Figure 2b relative to (2a). At the same time, cloud feedbacks in low- and mid-latitudes as shown in Figures 1c and 1d manifest themselves in the all-sky albedo time series.

[28] Having explored the climate change signals in broadband albedo, we can compare the above results with those where time series analysis is performed with spectral albedo and nadir spectral reflectance records from the OSSE experiment. Differences in detection times could arise from the spectral and geometrical integrations required to calculate broadband albedo from spectral radiances. The rationale for first applying detection analysis to spectral albedo and then to nadir spectral reflectance is to deconvolve their spectral and geometrical factors. The effects of spectral integration on detection times can by isolated by comparing the times for changes in spectral and broadband albedos. Likewise, the effects of geometrical integration are quantified by comparing the times computed for spectral albedos and nadir reflectances. It should be noted that estimates of spectral albedo are challenging to obtain from satellite instruments [e.g., *Privette et al.*, 1997] and the current design of CLARREO does not specify such measurements. Qualitatively, there will likely be more information in spectrally resolved measurements as compared to the broadband, but it remains an open question as to whether this information can be used to hasten the detection of climate system changes such as those associated with the A2 emissions scenario.

[29] To illustrate where spectral measurements may provide more information over broadband measurements, Figures 3a–3e shows the anomaly time series for zonally averaged broadband albedo, spectral albedo, and nadir spectral reflectance at a single latitude (in this case, for 20 N) relative to mean values from the simulation for the 2000–2009 decade. The plot in Figure 3a is familiar in that the lines represent a transect of the information presented in Figures 2a and 2b. However, the spectral albedo and nadir reflectance plots provide an indication that there are several competing effects. In Figures 3b and 3d which indicate the clear sky time series of spectral albedo and nadir reflectance, respectively, we can see the influence of the time series of aerosol forcing in the window portions of the visible and near-infrared spectra, all of which increase for the first half of the 21st Century and then return to the zero anomaly level by the end of the Century. However, the water vapor feedback contained as shown in Figure 1b increases the column water vapor amount considerably in the second half of the 21st Century, and this is manifested in the darkening of the water vapor overtone bands. The features in these bands explain the clear-sky broadband albedo decrease between 2065 and 2100 at this latitude shown in Figure 3a.

[30] The all-sky albedo time series shows considerable interannual variability, mostly resulting from 2-year ENSO events [*Collins et al.*, 2006a], but this time series exhibits a notable and increasing secular trend as a result of increasing low-cloud amount. The time series of all-sky spectral albedo and nadir reflectance indicate the combined influence of

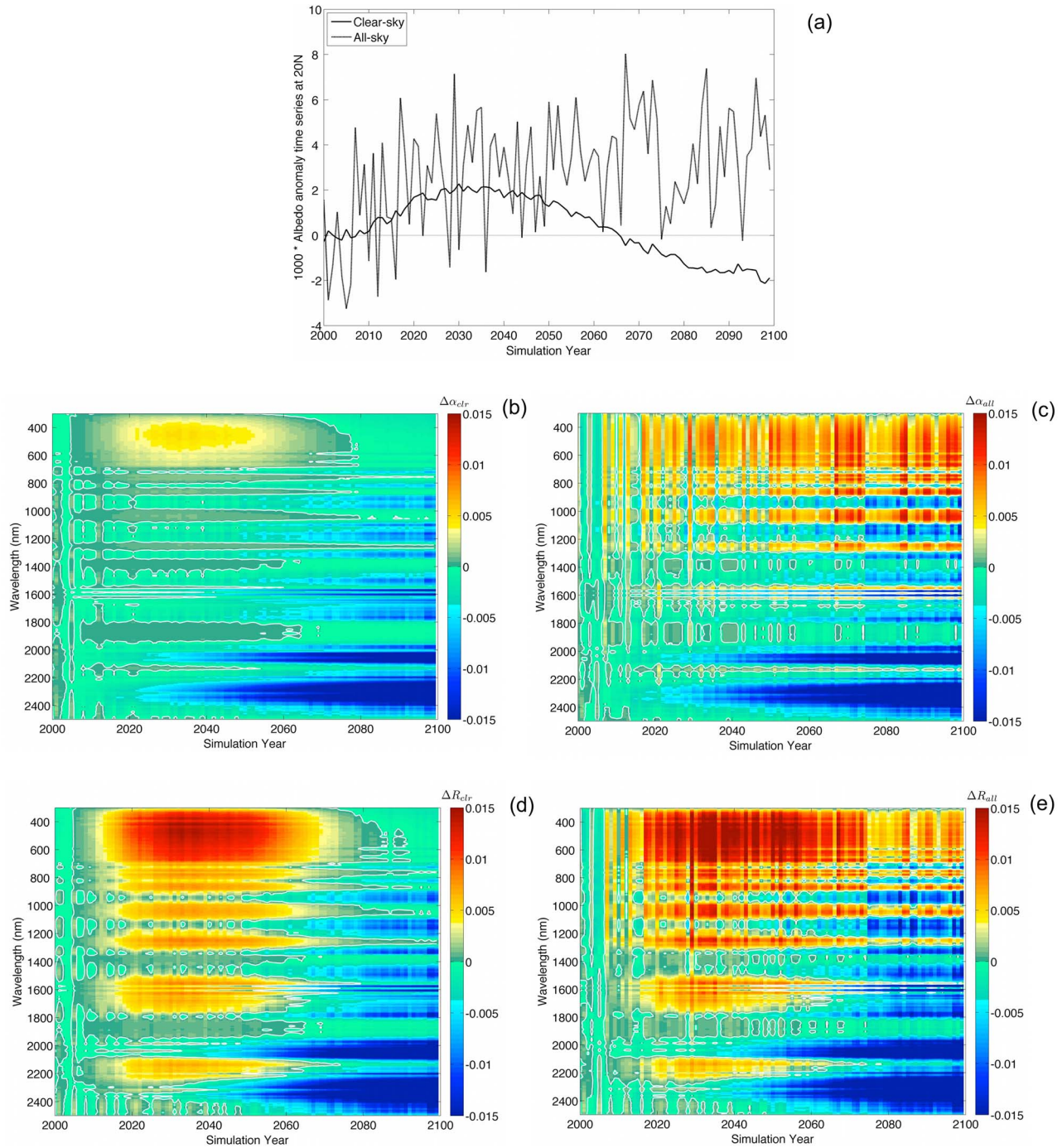

Figure 3. (a) Clear-sky and all-sky broadband zonally and annually averaged albedo anomaly time series at 20N. (b) Clear-sky spectral zonally and annually averaged albedo anomaly time series at 20N. (c) Same as Figure 3b but for all-sky conditions. (d) Same as Figure 3b but showing the spectral reflectance anomaly time series. (e) Same as Figure 3d but for all-sky conditions. For all plots, white contours denote zero difference line.

aerosol increases and increases in stratus clouds in this region that lead to increased albedo and nadir reflectance in the visible window channels. The spectral features of both aerosols and stratus clouds are more separable in the near-infrared window channels. This can be seen by comparing the increases in the clear-sky and all-sky spectra and noting that that increases in clear-sky nadir reflectance are higher in window bands at shorter wavelengths than in window bands at longer wavelengths, while the increases in nadir all-sky spectral reflectance exhibits less spectral structure between 300 and 1300 nm. This distinguishing feature arises because of the difference in angstrom exponent between the aerosols

and the clouds. Similar to the clear-sky plots, the all-sky spectral albedo and nadir reflectance plots also show decreases in the water vapor overtone bands, indicating the role of this gas in reducing broadband albedo by the end of the 21st Century. From these plots, it is apparent that there is considerably more structure in the spectral plot when one considers the extent to which different spectral intervals have opposite trend signs. For a given latitude, the spectral features where opposite trends are present are indicative of forcing and feedback mechanisms that will be obscured by a single broadband measurement.

[31] Figures 4a and 4b show the estimates of the time required to confidently detect a change in zonally averaged clear- or all-sky albedo with a perfect observing system as derived in equation (9). Under clear-sky conditions, the increase in aerosols in the A2 climate-change scenario is detectible with 5 years' of albedo measurements in lower and mid latitudes. However, the edges of the snowpack at northern midlatitudes and sea-ice extent at northern and southern high-latitudes have a large amount of interannual variability that precludes change detection except for multi-decadal data records. At the highest southern latitudes, there is very little interannual variability in snow and ice coverage both of which change very little despite the climate forcings. There is considerably more interannual variability in all-sky albedo change time series at most latitudes with secular trends generally emerging in the middle to end of the 21st Century at most latitudes, though robust trend detection is still very challenging at low latitudes even at 50- to 60-year timescales. However, the zonally averaged albedo changes associated with the movement of the stratus regions and midlatitude storm-tracks would be detectable within 20 years. For a few latitudes (i.e., 30 S and 70 S), the time series of all-sky broadband albedo has either a small secular trend or a large amount of natural variability, and the change detection time is indeterminate with the length of the record which is indicated where the detection time line increases to the length of the time series.

[32] We can also explore the utility of single spectral channel measurements. Figures 4c and 4d show the zonally and annually averaged time series of spectral albedo for a channel from 546 to 554 nm for clear-sky and all-sky conditions, respectively. The superimposed black line again indicates the change detection time as determined using equation (9). The time series very closely resemble those of their respective broadband albedo time series.

[33] Meanwhile, the time series of nadir spectral reflectance indicates that aerosols produce a more significant signal for the nadir spectral reflectance as compared to the spectral albedo due to the anisotropicity of the scattering produced by the aerosol particles with more scattering in the backscatter direction as compared to the hemispheric average. The time series of nadir clear-sky reflectance anomalies in a channel spanning from 546 to 554 nm, as seen in Figure 4e, shows a more pronounced signal from the increase in aerosol loading, but the time required to detect change differs very little between the spectral albedo plot of Figure 4c and the nadir spectral reflectance plot of Figure 4e. The nadir all-sky spectral reflectance plot in Figure 4f shows a more pronounced aerosol signal superimposed upon trends in cloud features with change detection achieved within 10–20 years at latitudes between 50 S and 50 N. The difference between the affect of aerosols on spectral albedo in Figure 4c and spectral reflectance in Figure 4f is due to the phase function of the aerosols in the OSSE. The aerosol phase function, derived from Mie theory, displays a higher aerosol backscatter in a nadir-viewing instrument at low-latitudes relative to the total backscatter fraction that governs the signal of aerosols in an albedo measurement.

[34] The signal from aerosols is more muted in Figure 4g with the time series of nadir clear-sky spectral reflectance from a channel spanning a weak water vapor overtone feature from 936 to 944 nm as compared to the 550 nm channel. However, the nadir all-sky reflectances, as displayed in Figure 4h, which are insensitive to low clouds but sensitive to high clouds, shows that movement of the ITCZ can be detected with a measurement record between 20 and 40 years in length.

[35] To address the extent to which zonal and annual averaging are biasing our estimates of the times to detection for climate change trends, we have analyzed temporal and spatial subsets of the OSSE data in Figures 5a–5d. In particular, we have separately calculated the change detection time for seasonal subsets of the data as shown in Figure 5a. The detection times derived using seasonal averages are generally similar to those derived using annual averages except for boreal summer conditions at around 40N, where interannual variability in snow coverage significantly lengthens the detection time for analysis based on annual averages. For all-sky conditions as shown in Figure 5b, the year-to-year variability in seasonal cloud coverage is generally more significant than the variability in annual averages, so annual average analysis is warranted. Some of the principal sources of unforced variability in nadir spectral reflectance are from sea-ice and snow, which affect albedos for oceanic and terrestrial regions, respectively. Since unforced variability is one of the major factors that increase trend detection times as shown in equation (6), we have also tested whether the trend detection times for broadband albedos zonally averaged over all surface types differ from those for separate averages over land and ocean regions. In Figures 5c and 5d, we contrast the detection times for all surfaces and land regions, and ocean regions under clear-sky and all-sky conditions. Under most circumstances, detection times for land and ocean scenes analyzed separately are longer than a land-ocean zonal average, especially in the midlatitude

Figure 4. (a) Zonally and annually averaged time series of changes in broadband albedo for clear-sky conditions with a black line superimposed to indicate the running-estimate of change detection time at each latitude for the clear-sky time series. (b) Same as Figure 4a but for all-sky conditions. (c) Same as Figure 4a but for spectral albedo over the band from 545 and 555 nm between each year of the simulation and the time-mean zonally averaged albedo during 2000–2009 for clear-sky conditions. (d) Same as Figure 4c but for all-sky conditions. (e) Same as Figure 4a but the time series corresponds to spectral clear-sky reflectance difference over the band from 545 and 555 nm. (f) Same as Figure 4e but for all-sky reflectance. (g) Same as Figure 4e but covering the band from 935 to 945 nm. (h) Same as Figure 4f but covering the band from 935 to 945 nm. For all plots, white contours denote zero difference line.

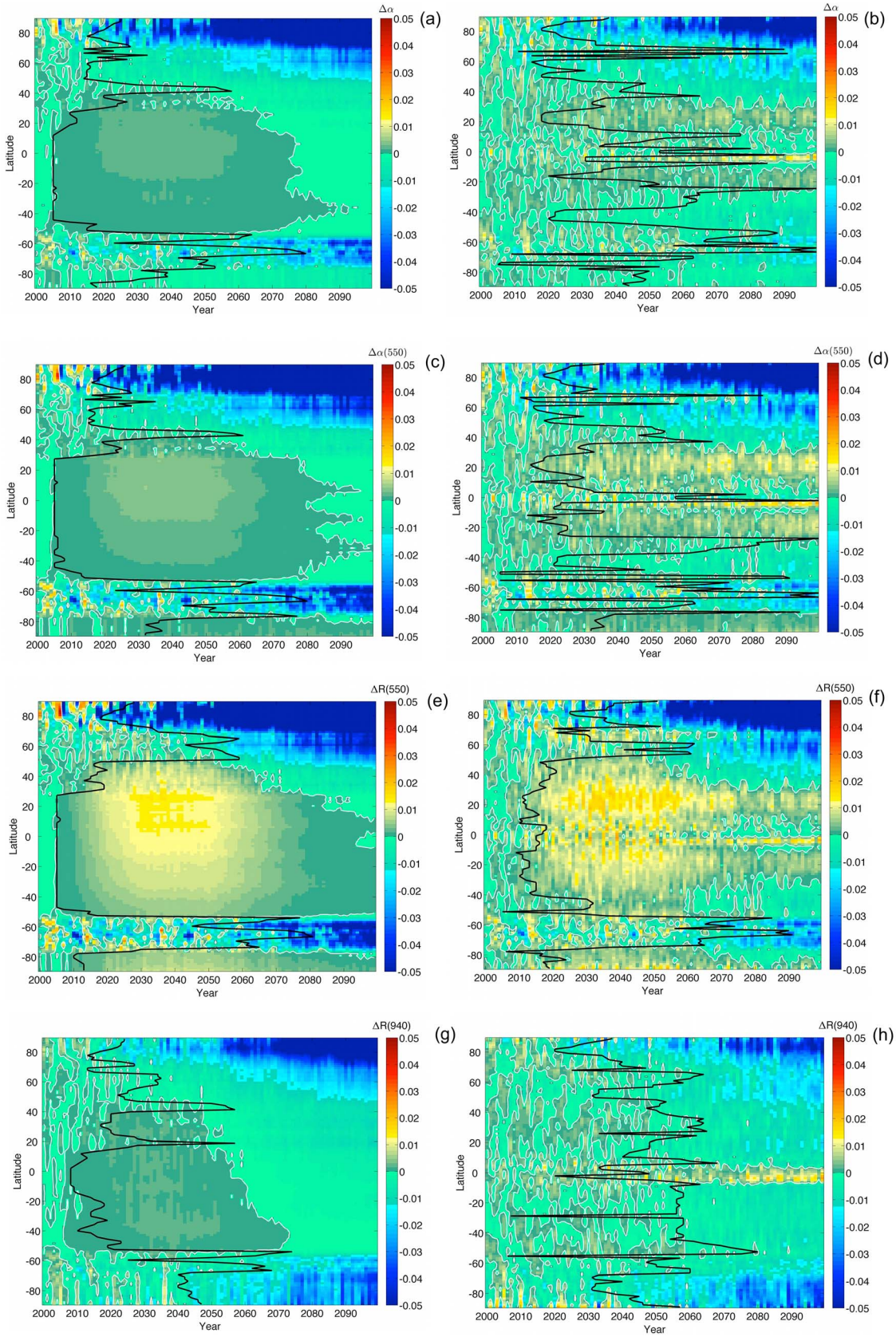
(a)
(b)
(c)
(d)
(e)
(f)
(g)
(h)
Δα
Δα(550)
ΔR(550)
ΔR(940)
Latitude
Year
80
60
40
20
0
-20
-40
-60
-80
2000
2010
2020
2030
2040
2050
2060
2070
2080
2090
0.05
0.04
0.03
0.02
0.01
0
-0.01
-0.02
-0.03
-0.04
-0.05

Figure 4

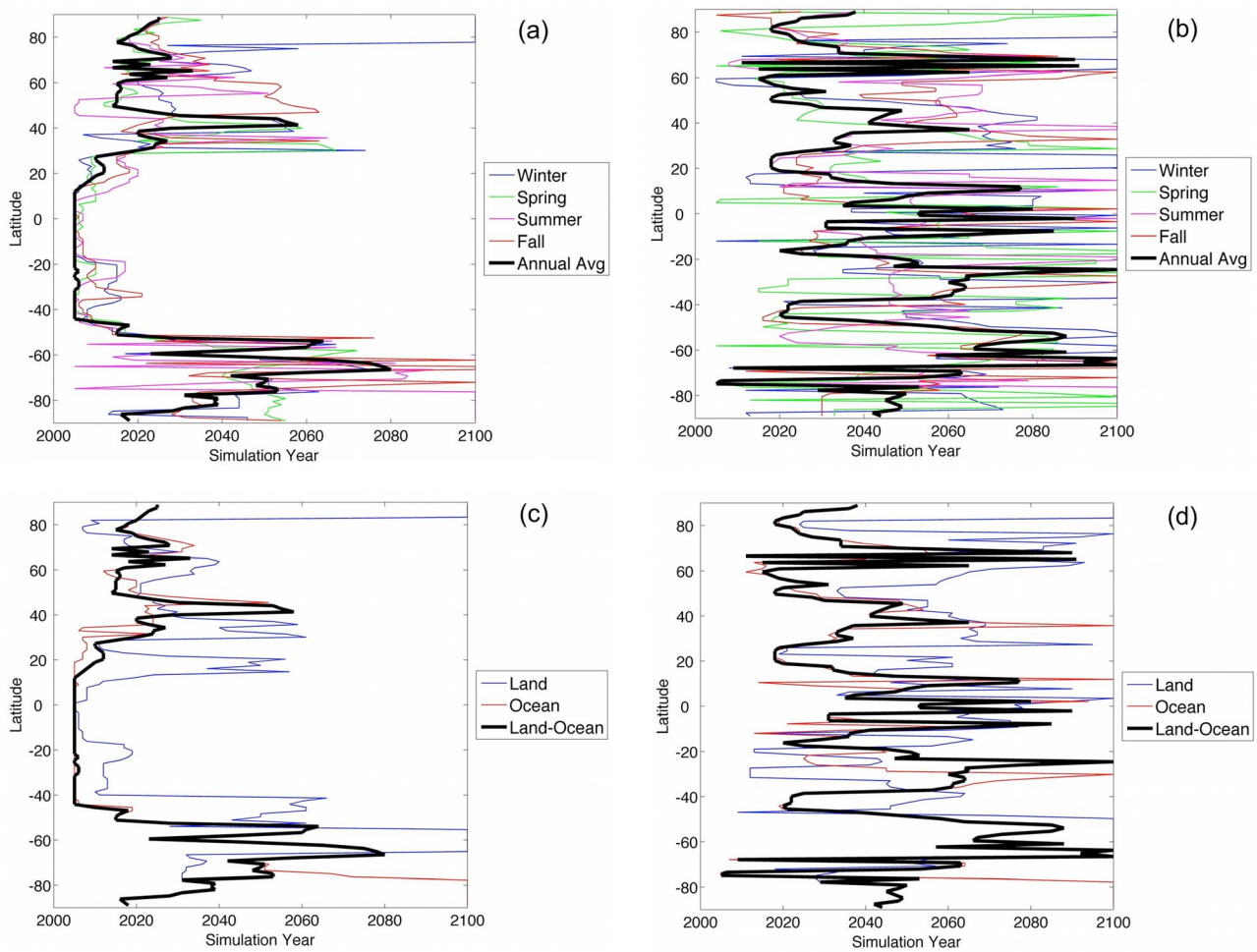

Figure 5. (a) Clear-sky detection times for zonally averaged albedo from 12-month annual, boreal winter (December, January, and February), spring (March, April, and May), summer (June, July, and August), and fall (September, October, and November) averages. (b) Same as Figure 5a but for all-sky conditions. (c) Clear-sky detection times for albedo derived from zonal averages (land-ocean), zonal averages of land scenes only, and zonal averages of ocean scenes only. (d) Same as Figure 5c but for all-sky conditions.

regions where snow cover variability is significant but variable.

[36] Detection of change for spectrally resolved signals can be approached with a variety of different methods, but for the purposes of this preliminary analysis, we assume that the spectral channels are uncorrelated. We recognize that spectral channels are indeed correlated and that the assumption that they are not correlated may lengthen detection times; therefore, it is expected that actual spectral measurements will perform better than the results shown here if the independent and correlated information in the spectra is analyzed properly. In Figures 6a–6d, we compare the detection time associated spectral albedo and nadir reflectance. The figures show patches of color and patches of white. Where color is displayed, the detection time for spectral albedo or nadir reflectance is less than that for broadband albedo. Where patches of white are displayed, the detection time for the spectral measurements is longer than that of broadband measurements. This figure shows that the spectral data contain a considerable amount of value relative to broadband measurements. This value is expressed in several spectral regions. First, in the window channels in the nadir clear-sky reflectance spectra, many of the channels are sensitive to aerosol forcing. Under clear-sky conditions, the change detection time required for visible wavelengths is considerably less than 10 years and comparable to a satellite mission lifetime, due to aerosol loading along with limited natural variability. Moreover, changes in the edges of midlatitude snowpack can be discerned more quickly with many spectral albedo and nadir reflectance channels than broadband albedo.

[37] Nadir spectral reflectance measurements will also be important toward detecting changes in the cloud patterns that are projected to occur by the middle of the 21st Century, Figure 6d shows that these measurements will be especially useful in detecting changes in the superimposition of aerosol forcing with changes ITCZ and movement of the stratus regions faster than broadband measurements. Another feature that is apparent in Figure 6d is the utility of measurements between 2000 and 2500 nm in terms of fast change detection times. These window and weak water vapor channels are less sensitive to changes in frozen surface cover but

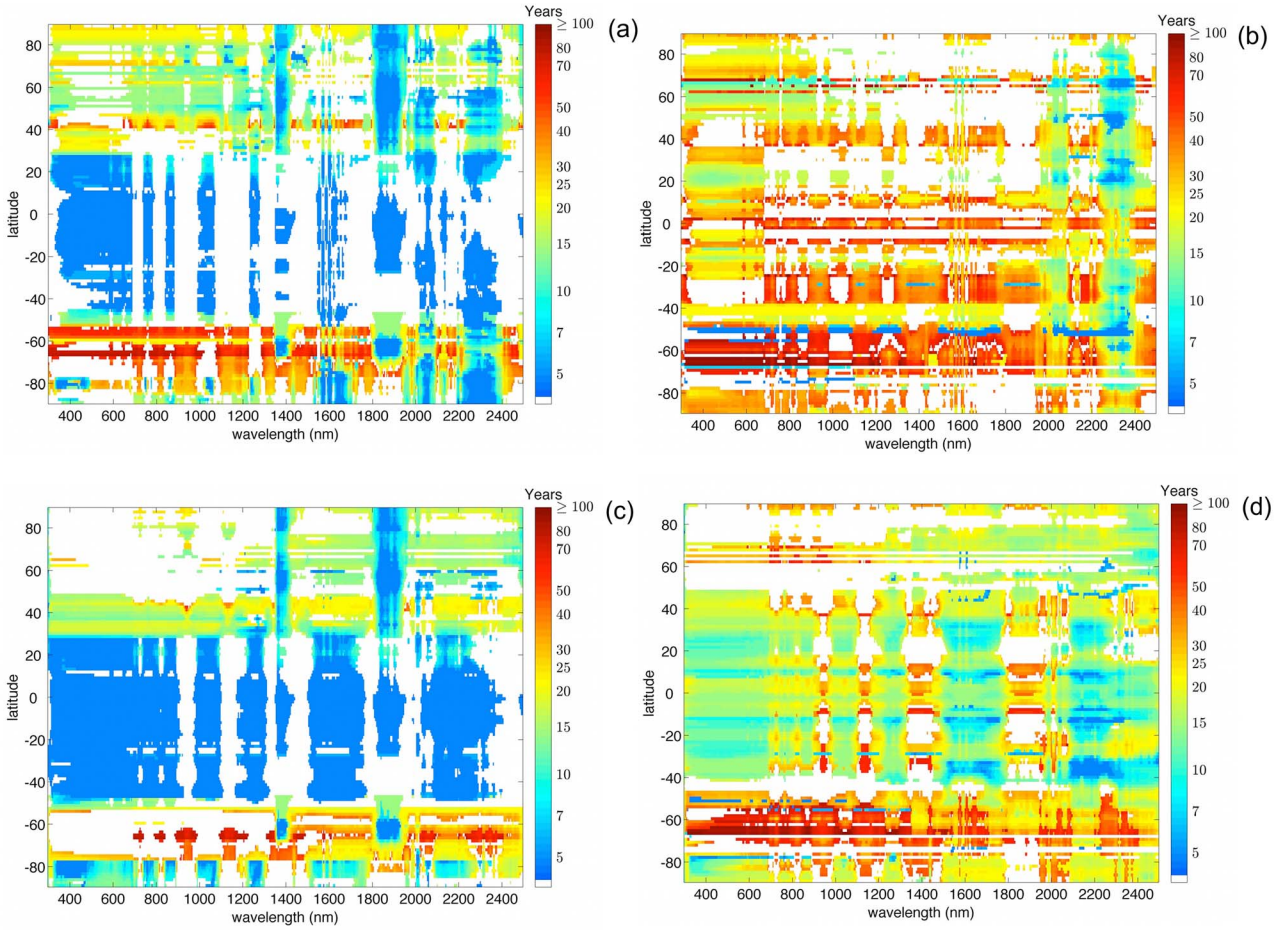

Figure 6. (a) Detection time for clear-sky zonally averaged spectral albedo measurements where the color indicates where such measurements are less than the detection time for the corresponding zonally averaged broadband albedo measurements. (b) Same as Figure 6a but comparing all-sky spectral albedo measurements with broadband albedo measurements. (c) Same as Figure 6a but comparing clear-sky spectral reflectance measurements with broadband albedo measurements. (d) Same as Figure 6a but comparing all-sky spectral reflectance measurements with broadband albedo measurements.

still partially sensitive to clouds and aerosols and may be useful for discerning between scenes where snow or sea-ice are changing and clouds are also changing. Changes in nadir all-sky spectral reflectance measurements in the visible bands at low latitudes and the near-IR bands at most latitudes may be detectable from a record around 30 years' in length.

[38] Despite the regions in Figures 6a–6d that indicate the utility of the instrument, there are several zonal and spectral regions for which no additional value is added by making nadir spectral reflectance measurements as opposed to broadband albedo measurements. This is largely true at high-latitude zones of snow and sea-ice change and those portions of the spectra with highly saturated water vapor bands. For the former conditions, the interannual variability in frozen surfaces affects certain shortwave spectral nadir reflectance channels more than broadband measurements, so broadband measurements are a better detector of secular trends. In the water vapor bands, the secular trend is very small compared to natural variability, particularly for the first half of the 21st Century, and change in these bands can only be detected after more than 50 years' of measurements.

[39] The information in Figures 6a–6d can be summarized in terms of a histogram of the detection time for spectral channels in detecting change relative to broadband albedo change detection. In Figure 7a, the distribution of spectral channel detection time shows that there are a significant number of spectral channels that can detect secular changes more quickly than with broadband measurements. The detection times for the nadir all-sky spectral reflectance channels shows that change can be detected in most spectral channels in 10 to 20 years except at the low-latitude edges of the snow- and sea-ice extent. These data can further be summarized by analyzing median detection times for nadir spectral reflectance and broad albedo in latitude bands, as shown in Table 1. This summary shows that the nadir spectral reflectance measurements allow for appreciably faster change detection for all-sky conditions at low and mid latitudes.

[40] The previous analyses were predicated on a detecting secular changes in data sets that were assumed to have no measurement uncertainty and to be free of artifacts. Using equation (10), we can relax this assumption and explore how imperfections in the observing system impact the time

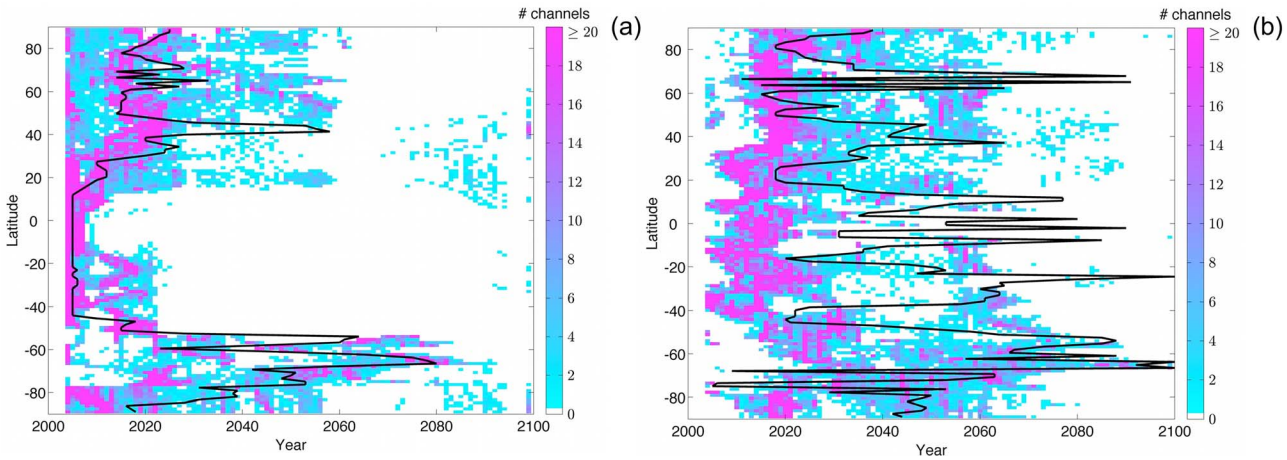

Figure 7. (a) A 2-D histogram of the spectral detection-times of the spectral reflectance channels shown in Figure 6c indicating the number of spectral channels with a given change detection time derived from the time series of zonally averaged clear-sky spectral reflectance. Superimposed with a black line is the change detection time from a time series of clear-sky broadband albedo. (b) Same as Figure 7a but the histogram values indicate change detection time based on all-sky spectral reflectance time series and the black line indicates the change detection time for an all-sky broadband albedo.

required to detect changes in the climate system. This total measurement uncertainty budget arises from several sources including calibration drift, incomplete spatiotemporal sampling, and reference intercalibration error. Qualitatively, accounting for imperfect instrumentation will lead to increased detection times, but this must be explored quantitatively because it has bearing on the utility of using existing instruments for change detection and on the prospects that future instrument specifications will be adequate for climate change detection. The specification for CLARREO measurement uncertainty currently is 0.3% (k = 2), which is equivalent to around 6×10^{-4} in reflectance units for each channel. From equation (10), we find that the ratio of measurement error to natural variability governs how detection time will increase.

[41] In Figure 8a, we can see that the zonally averaged change detection time for clear-sky broadband albedo measurements becomes indeterminate at low latitudes with measurement error above 5×10^{-4} (k = 1) in absolute albedo units (equivalent to around 0.35 W/m^2 k = 2). Since the current estimates of broadband measurement uncertainty for CERES is comparable to this value, total measurement error would be a limiting factor for clear-sky change detection for a climate forced by the A2 emissions scenario. Meanwhile, in Figure 8b, total measurement error for all-sky albedo measurements does lead to a small increase in the time required for change detection but the interannual variability in all-sky albedo is large compared to the measurement error. In Figure 8c, we perform a similar analysis as in Figure 8a but with nadir clear-sky spectral reflectance for a channel from 546 nm to 554 nm. Here, the change detection time at most latitudes does not increase appreciably for a total measurement error up to 6×10^{-4} in absolute reflectance units (equivalent to 0.3% k = 2). For measurement error greater than 6×10^{-4}, change detection with clear-sky measurements becomes indeterminate between 50S and 30N. As with Figure 8b, the impact of measurement error on all-sky reflectance for a channel spanning 546 to 554 nm is less than for clear-sky conditions because of the large interannual variability in all-sky reflectance at this wavelength. From Figures 8e and 8f, we can see that measurement error impacts change detection for a near-IR water vapor channel spanning 936 to 944 nm in a similar manner as the visible window channel. These findings suggest that the nominal instrument specification of 0.3% k = 2 at all wavelengths is warranted, especially for clear-sky measurements, and that a relaxation of this tolerance could prove detrimental to rapid detection of changes in spectral reflectance.

[42] In the following section, we explore how this data can be used to guide the analysis of existing data sets and development of novel ones.

4. Discussion

[43] Given the controversy associated with the determination of secular trends in long-term measurements of broadband

Table 1. Median Change Detection Time (in Years) for a Set of Latitude Bands of Zonally Averaged Clear- and All-Sky Broadband Albedo and Spectral Reflectance Measurements

	80°S–60°S	60°S–40°S	40°S–20°S	20°S–20°N	20°N–40°N	40°N–60°N	60°N–80°N
Median broadband clear-sky	52 years	17	5	5	20	16	19
Median spectral clear-sky	42	18	5	5	15	20	18
Median broadband all-sky	55	61	61	39	33	25	30
Median spectral all-sky	45	30	16	17	18	22	21

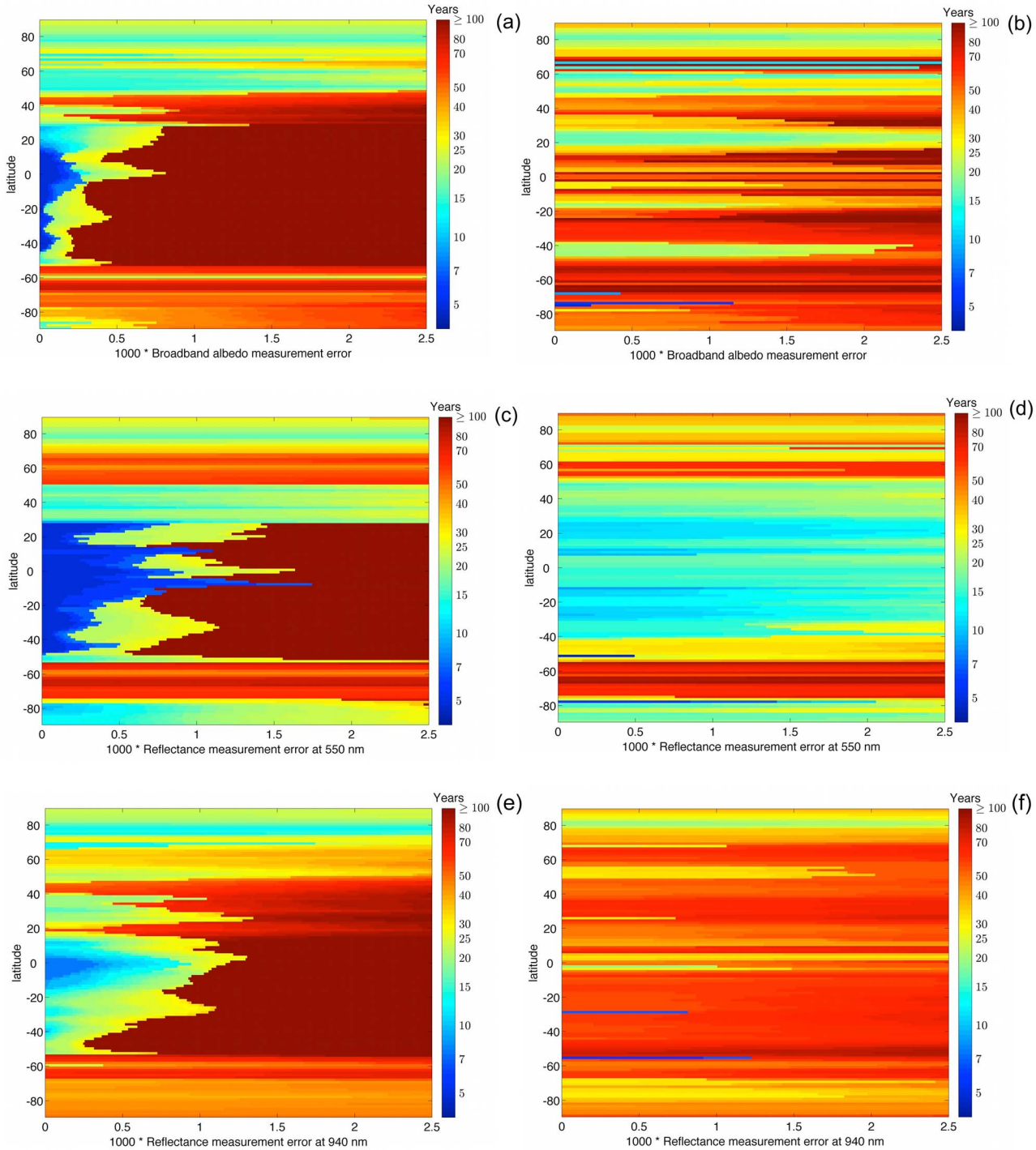

Figure 8. (a) All-sky detection time for zonally averaged broadband albedo versus latitude and measurement uncertainty (in absolute albedo units). (b) Same as Figure 8a but for clear-sky broadband albedo. (c) Same as Figure 8b but for all-sky spectral reflectance measurements at 550 nm and where measurement uncertainty is in absolute reflectance units. (d) Same as Figure 8c but for clear-sky spectral reflectance measurements. (e) Same as Figure 8c but for all-sky spectral reflectance measurements at 940 nm. (f) Same as Figure 8d but for clear-sky spectral reflectance measurements at 940 nm.

albedo data, this study has focused on detecting zonally averaged climate change signals in broadband albedo and nadir spectral reflectance measurements that have been simulated by a shortwave OSSE of the IPCC A2 scenario for the 21st Century [*IPCC*, 2000]. The goal of this research is to examine the relative utility of shortwave broadband albedo and nadir spectral reflectance measurements for detecting secular trends in the climate system that result either directly

from the prescribed forcings of the emissions scenario or indirectly from climate system feedbacks. The analysis of long-term synthetic data presented here shows that secular trends associated with broadband and spectral measurements are quite spatially variable. Nevertheless, the results show that under certain conditions (e.g., clear-sky tropical scenes), secular changes in broadband albedo and visible-channel nadir spectral reflectance can be identified in a 5-year data set, a period comparable to the duration of typical satellite instruments. The results also show that secular change detection requires decades of broadband measurements in zones of large variability such as the midlatitude edges of snow coverage and sea-ice extent. The variability in cloud cover tends to lead to significantly longer change detection times due to larger interannual variability in zonally averaged cloud cover, but all-sky spectral reflectance measurements at low latitudes may be used to detect secular change much faster than with broadband albedo data.

[44] Spectral measurements may enable much faster detection of changes relative to broadband measurements due to the existence of spectral bands with large trends but opposing signs that partially cancel one another in broadband signals. In the presence of both natural variability and instrumental noise, the visible channels, in particular, provide much faster detection time than broadband measurements, and this analysis has found that uncertainty in broadband albedo measurements plays a significant role in lengthening the time required to detect secular changes in that quantity. All-sky nadir spectral reflectance measurements will facilitate the detection of changes in the ITCZ and stratus regions more rapidly than would be possible with broadband measurements, with change detection achieved with a data record of approximately 20 years. By simultaneously tracking changes in window channels across the visible and near-infrared portions of the spectrum and also measuring water vapor overtone bands, spectral measurements are capable of distinguishing between those aspects of the climate system that directly lead to changes in broadband albedo. This work has shown that the climate change prescribed in the A2 emissions scenario can be detected earlier with some spectral measurements as compared to broadband measurements, due to the fact that the broadband measurements integrate over a combination of secular features, some of which change rapidly (i.e., aerosol loading), and others which change more slowly (i.e., water vapor and cloud feedbacks).

[45] We should note that the findings regarding measurement uncertainty suggest that this quantity, and not natural variability, may be a limiting factor for change detection. In particular, we find that under circumstances with time-varying forcing terms, such as those prescribed by the A2 aerosol emissions scenario, a small amount of measurement uncertainty can render the secular change detection problem indeterminate. Therefore, measurement uncertainty must be considered carefully in the analysis of long-term data records both from broadband and spectral measurements.

[46] While there are many statistical techniques that can be employed to analyze OSSE data, the straightforward methods that we have employed here have been used extensively for climate change signal analysis [e.g., *Chen et al.*, 2002; *Reinsel et al.*, 2005; *Soden et al.*, 2005] and are useful for gauging the utility of broadband albedo and nadir spectral reflectance measurements for estimating change detection.

[47] There are, however, several caveats to the results presented here that arise both from the analysis methods and from the OSSE formulation. In terms of the methods used for statistical analysis, we started with a method to partition the data time series into a secular linear signal and a time-invariant noise process. This approach is useful for conducting preliminary analyses, but is deficient for systems where the secular signals are nonlinear and/or the noise process is non-stationary. For example, the change in sign in the secular trends in anthropogenic aerosols in the IPCC A2 scenario complicates the change detection algorithm, and this creates a situation where the length of data record required for detecting change increases with the length of the record. Also, the working assumption made in this paper that the spectral channels are uncorrelated needs to be relaxed. Detection of trends in coherent spectral bands should be much more robust than detection with single channels due to the statistical suppression of random instrumental noise in the spectral summation process, and hence it is likely that the detection times for changes in coherent spectral bands will be appreciably shorter than the times reported here for individual channels. Finally, much of the discussion in this paper talks about the detection of changes in signals and ascribes those changes to underlying features of the climate system. Formal attribution methods [e.g., *Leroy et al.*, 2008b] are outside of the scope of this initial analysis but will be undertaken next in order to advance our understanding of prospective climate change signals in nadir shortwave reflectances.

[48] Another important caveat is that because results regarding the utility of a proposed instrument based on OSSEs are predicated on how realistic the underlying inputs are, any statements made about the benefit of the instrument in question likely represent a best-case scenario. Because the simulations are a simplification of the actual climate system, the findings herein are warranted insofar as the natural variability in processes that affect spectral and broadband measurements is realistically described in the CCSM3 model. Comparisons between all-sky spectra from the SCIAMACHY satellite instrument [*Bovensmann et al.*, 1999] and the OSSE spectra for present-day conditions suggest that the natural variability in the OSSE may indeed be realistic. Figures 9 and 10 shows a comparison of the principal components (PCs) derived from SCIAMACHY and data from the OSSE control run for October, 2004. This example shows close agreement in some aspects of the spectral variance in both data sets. The data variance contribution shown in Figure 9 indicates that the OSSE is underestimating the contribution of the first PC that has been ascribed to cloud reflectance [*Roberts et al.*, 2011] but also indicates close agreement in variance contribution of the lower-order PCs. Furthermore, the consistency in spectral shape agreement in Figure 10 for the first 5 PCs indicates that the OSSE data and SCIAMACHY data are quite similar in terms of the contributions to data set variability. Still, there are open questions about how realistic the variability is in the OSSE by the middle or end of the 21st Century where significant climate change will have occurred. We expect that the statistics associated with the sea-ice extent and snow fraction will be non-stationary in the face of fundamental changes in cryospheric coverage. The statistics associated with the migration of storm tracks and strengthening of stratus clouds also may be non-stationary.

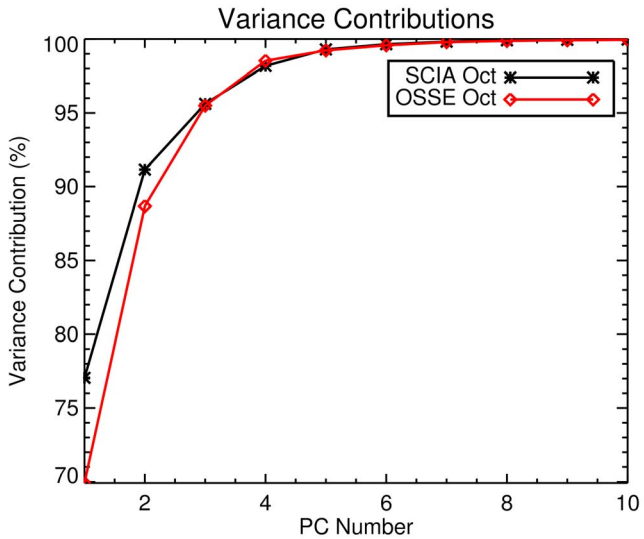

Figure 9. The cumulative variance contribution of the first 10 principal components derived from SCIAMACHY data from October 2004 and data from the OSSE control run for the same time period.

[49] Future research regarding the analysis of nadir shortwave reflectance simulations should expand beyond the treatment of zonal and annual averages and focus on identifying signals separately on the land and ocean and on a seasonal basis. Also, key questions regarding measurement sampling errors have not been discussed here but are critical for determining the ultimate utility of shortwave spectral measurements. Further simulations at high temporal resolution to capture the diurnal cycle or over different satellite orbits may be required to address the magnitude of systematic errors associated with low-earth orbit sampling relative to a perfect observing system for shortwave spectral reflectance. Previous work by *Kirk-Davidoff et al.* [2005] may provide a useful starting point for this analysis. Nevertheless, it is hoped that this analysis will provide a starting point for the discussion of the role of nadir spectral reflectance measurements in tracking trends in planetary albedo and enabling early change detection in this quantity.

[50] Last, in the same way that albedo changes are not independent of changes in the outgoing longwave radiation, the analysis of observational simulations of nadir shortwave reflectance is incomplete without looking at both shortwave and longwave spectra. Pan-spectral methods will be critical both to gauge the spectral signatures of climate change

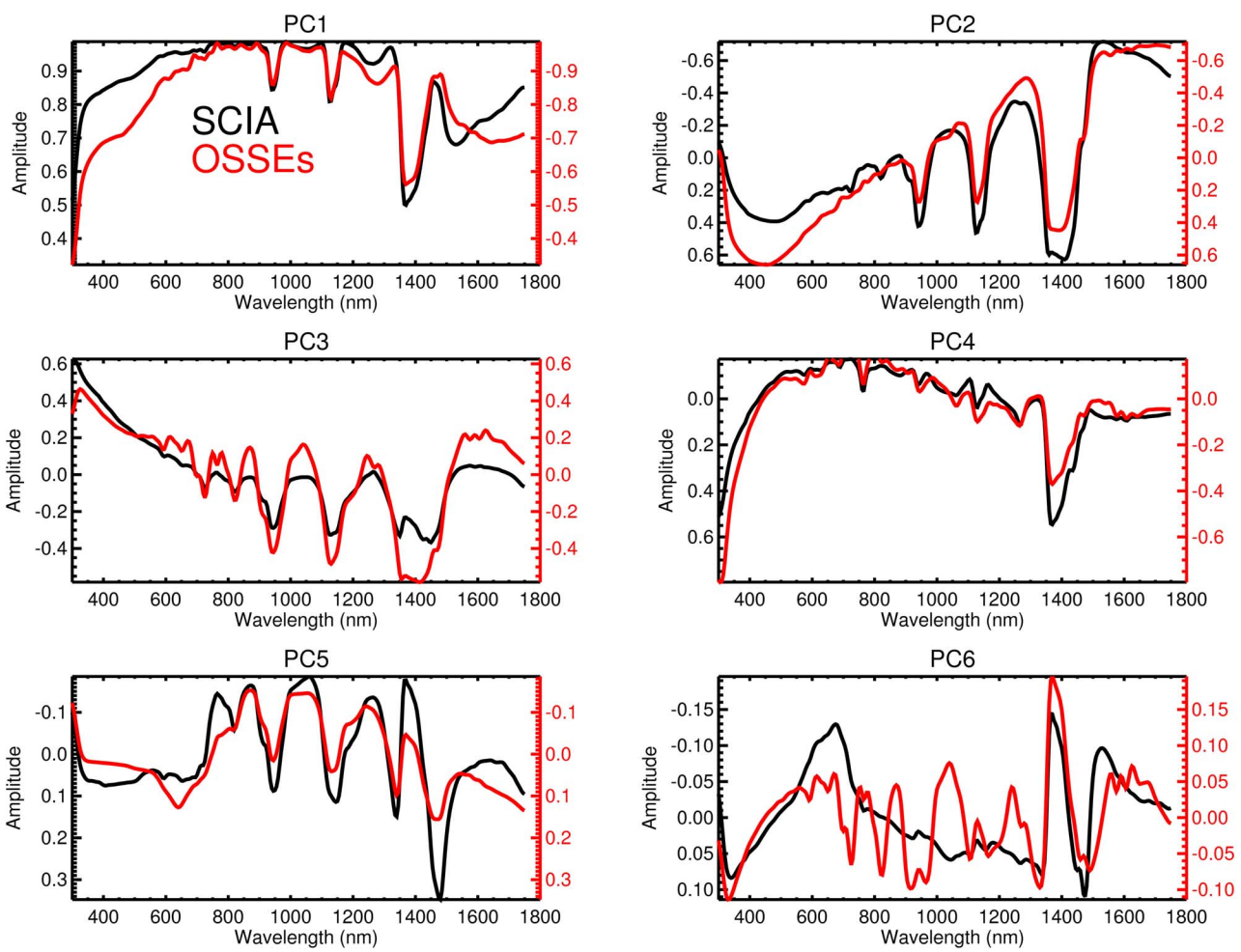

Figure 10. A comparison of the first 6 spectral principal component vectors for data from SCIAMACHY and the OSSE.

feedbacks and to determine what is being missed where only one of these spectral ranges is being measured.

[51] **Acknowledgments.** Funding for this research was supported by the following NASA grants: NNX08AT80G, NAS2–03144, NNX10AK27G, and NNX11AE65G. This work was also supported by Contractor Supporting Research (CSR) funding from Berkeley Lab, provided by the Director, Office of Science, of the U.S. Department of Energy under contract DE-AC02-05CH11231. Additionally, NASA High-End Computing grants SMD-08-0999, SMD-09-1397, and SMD-10-1799 allotted computational resources to produce the simulations. The following individuals also provided considerable assistance with this research: Stephen Leroy and Yi Huang of Harvard University, David Young, Bruce Wielicki, Zhonghai Jin, and Rosemary Baize of the NASA Langley Research Center, Chris Paciorek, Jonathan Ong, and Michael Dreibelbis of the University of California-Berkeley, Chris Little and Tsengdar Lee of the NASA Science Mission Directorate, and the entire NASA High-End Computing technical support team of NASA User Services.

References

Anderson, J., J. Dykema, R. Goody, H. Hu, and D. Kirk-Davidoff (2004), Absolute, spectrally resolved, thermal radiance: A benchmark for climate monitoring from space, *J. Quant. Spectrosc. Radiat. Transfer*, *85*(3–4), 367–383, doi:10.1016/S0022-4073(03)00232-2.

Barkstrom, B. R., and G. L. Smith (1986), The Earth Radiation Budget Experiment: Science and implementation, *Rev. Geophys.*, *24*(2), 379–390, doi:10.1029/RG024i002p00379.

Berk, A., et al. (1999), MODTRAN4 radiative transfer modeling for atmospheric correction, *Proc. SPIE Int. Soc. Opt. Eng.*, *3756*, 348–353.

Bovensmann, H., et al. (1999), SCIAMACHY: Mission objectives and measurement modes, *J. Atmos. Sci.*, *56*(2), 127–150, doi:10.1175/1520-0469(1999)056<0127:SMOAMM>2.0.CO;2.

Briegleb, B. P., C. M. Bitz, E. C. Hunke, W. H. Lipscomb, M. M. Holland, J. L. Schramm, and R. E. Moritz (2004), Scientific description of the sea ice component in the Community Climate System Model, Version Three, *NCAR Tech. Rep. NCAR/TN-463+STR*, 78 pp., Natl. Cent. for Atmos. Res., Boulder, Colo.

Chen, J., B. E. Carlson, and A. D. Del Genio (2002), Evidence for strengthening of the tropical general circulation in the 1990s, *Science*, *295*(5556), 838–841, doi:10.1126/science.1065835.

Collins, W. D., et al. (2004), Description of the NCAR Community Atmosphere Model (CAM 3.0), *NCAR Tech. Note. NCAR/TN-464+STR*, 226 pp., Natl. Cent. for Atmos. Res., Boulder, Colo.

Collins, W. D., et al. (2006a), The Community Climate System Model: CCSM3, *J. Clim.*, *19*, 2122–2143, doi:10.1175/JCLI3761.1.

Collins, W. D., et al. (2006b), The formulation and atmospheric simulation of the Community Atmosphere Model: CAM3, *J. Clim.*, *19*, 2144–2161, doi:10.1175/JCLI3760.1.

Dickinson, R. E., K. W. Oleson, G. Bonon, F. Hoffman, P. Thornton, M. Vertenstein, Z. L. Yang, and X. Zeng (2006), The Community Land Model and its climate statistics as a component of the Community Climate System Model, *J. Clim.*, *19*, 2302–2324, doi:10.1175/JCLI3742.1.

Ducet, N., P.-Y. Le Traon, and G. Reverdin (2000), Global high resolution mapping of ocean circulation from TOPEX/Poseidon and ERS-1 and -2, *J. Geophys. Res.*, *105*(C8), 19,477–19,498, doi:10.1029/2000JC900063.

Feldman, D. R., C. A. Algieri, J. R. Ong, and W. D. Collins (2011), CLARREO shortwave observing system simulation experiments of the twenty-first century: Simulator design and implementation, *J. Geophys. Res.*, *116*, D10107, doi:10.1029/2010JD015350.

Goody, R. M., J. G. Anderson, and G. North (1998), Testing climate models: An approach, *Bull. Am. Meteorol. Soc.*, *79*(11), 2541–2549, doi:10.1175/1520-0477(1998)079<2541:TCMAA>2.0.CO;2.

Harries, J. E., H. E. Brindley, P. J. Sagoo, and R. J. Bantges (2001), Increases in greenhouse forcing inferred from the outgoing longwave radiation spectra of the Earth in 1970 and 1997, *Nature*, *410*, 355–357, doi:10.1038/35066553.

Haskins, R. D., R. M. Goody, and L. Chen (1997), A statistical method for testing a general circulation model with spectrally resolved satellite data, *J. Geophys. Res.*, *102*(D14), 16,563–16,581, doi:10.1029/97JD00897.

Huang, Y., and V. Ramaswamy (2009), Evolution and trend of the outgoing longwave radiation spectrum, *J. Clim.*, *22*, 4637–4651, doi:10.1175/2009JCLI2874.1.

Huang, Y., S. Leroy, P. J. Gero, J. Dykema, and J. Anderson (2010), Separation of longwave climate feedbacks from spectral observations, *J. Geophys. Res.*, *115*, D07104, doi:10.1029/2009JD012766.

Hurrell, J. W., and K. E. Trenberth (1998), Difficulties in obtaining reliable temperature trends: Reconciling the surface and satellite microwave sounding unit records, *J. Clim.*, *11*, 945–967, doi:10.1175/1520-0442(1998)011<0945:DIORTT>2.0.CO;2.

Intergovernmental Panel on Climate Change (IPCC) (2000), *Special Report on Emissions Scenarios: A Special Report of Working Group III of the Intergovernmental Panel on Climate Change*, edited by N. Nakicenovic et al., 599 pp., Cambridge Univ. Press, Cambridge, U. K.

Intergovernmental Panel on Climate Change (IPCC) (2007), *Climate Change 2007: The Physical Science Basis. Contribution of Working Group I to the Fourth Assessment Report of the Intergovernmental Panel on Climate Change*, edited by S. Solomon et al., Cambridge Univ. Press, Cambridge, U. K.

Justice, C. O., et al. (1998), The Moderate Resolution Imaging Spectroradiometer (MODIS): Land remote sensing for global change research, *IEEE Trans. Geosci. Remote Sens.*, *36*, 1228–1249, doi:10.1109/36.701075.

Kiehl, J. T., C. A. Shields, J. J. Hack, and W. D. Collins (2006), The climate sensitivity of the Community Climate System Model Version 3 (CCSM3), *J. Clim.*, *19*, 2584–2596, doi:10.1175/JCLI3747.1.

Kirk-Davidoff, D. B., R. M. Goody, and J. G. Anderson (2005), Analysis of sampling errors for climate monitoring satellites, *J. Clim.*, *18*, 810–822, doi:10.1175/JCLI-3301.1.

Kopp, G., P. Pilewskie, G. Drake, J. Espejo, D. Harber, K. Heuerman, and Y. Roberts (2009), Short-wave instrument development for CLARREO, paper presented at Hyperspectral Imaging and Sensing of the Environment, Clim. Absolute Radiance and Refractivity Obs., Vancouver, B. C., Canada.

Leroy, S. S., J. G. Anderson, and G. Ohring (2008a), Climate signal detection times and constraints on climate benchmark accuracy requirements, *J. Clim.*, *21*, 841–846, doi:10.1175/2007JCLI1946.1.

Leroy, S. S., J. G. Anderson, J. Dykema, and R. Goody (2008b), Testing climate models using thermal infrared spectra, *J. Clim.*, *21*, 1863–1875, doi:10.1175/2007JCLI2061.1.

Loeb, N. G., B. A. Wielicki, D. R. Doelling, G. L. Smith, D. F. Keyes, S. Kato, N. Manolo-Smith, and T. Wong (2009), Toward optimal closure of the Earth's top-of-atmosphere radiation budget, *J. Clim.*, *22*, 748–766, doi:10.1175/2008JCLI2637.1.

Meehl, G. A., W. M. Washington, W. D. Collins, J. M. Arblaster, A. Hu, L. E. Buja, W. G. Strand, and H. Teng (2005), How much more global warming and sea level rise?, *Science*, *307*, 1769–1772, doi:10.1126/science.1106663.

Meehl, G. A., et al. (2006), Climate change projections for the twenty-first century and climate change commitment in the CCSM3, *J. Clim.*, *19*, 2597–2616, doi:10.1175/JCLI3746.1.

Pallé, E., P. R. Goode, P. Montanes-Rodriguez, and S. E. Koonin (2004), Changes in Earth's reflectance over the past two decades, *Science*, *304*(5675), 1299–1301, doi:10.1126/science.1094070.

Pallé, E., P. R. Goode, and P. Montanes-Rodriguez (2009), Interannual variations in Earth's reflectance 1999–2007, *J. Geophys. Res.*, *114*, D00D03, doi:10.1029/2008JD010734.

Pearlman, J. S., P. S. Barry, C. C. Segal, J. Shepanski, D. Beiso, and S. L. Carman (2003), Hyperion, a space-based imaging spectrometer, *IEEE Trans. Geosci. Remote Sens.*, *41*(6), 1160–1173, doi:10.1109/TGRS.2003.815018.

Privette, J. L., T. F. Eck, and D. W. Deering (1997), Estimating spectral albedo and nadir reflectance through inversion of simple BRDF models with AVHRR/MODIS-like data, *J. Geophys. Res.*, *102*(D24), 29,529–29,542, doi:10.1029/97JD01215.

Reinsel, G. C., A. J. Miller, E. C. Weatherhead, L. E. Flynn, R. M. Nagatani, G. C. Tiao, and D. J. Wuebbles (2005), Trend analysis of total ozone data for turnaround and dynamical contributions, *J. Geophys. Res.*, *110*, D16306, doi:10.1029/2004JD004662.

Roberts, Y. L., P. A. Pilewskie, and B. C. Kindel (2011), Evaluating the observed variability in hyperspectral Earth-reflected solar radiance, *J. Geophys. Res.*, doi:10.1029/2011JD016448, in press.

Schwartz, S. E., R. J. Charlson, R. A. Kahn, J. A. Ogren, and H. Rodhe (2010), Why hasn't Earth warmed as much as expected?, *J. Clim.*, *23*(10), 2453–2464, doi:10.1175/2009JCLI3461.1.

Soden, B. J., D. L. Jackson, V. Ramaswamy, M. D. Schwarzkopf, and X. Huang (2005), The radiative signature of upper tropospheric moistening, *Science*, *310*(5749), 841–844, doi:10.1126/science.1115602.

Space Studies Board (2007), *Earth Science and Applications from Space: National Imperatives for the Next Decade and Beyond*, 456 pp., Natl. Acad. Press, Washington, D. C.

Tashima, D. H., and D. L. Hartmann (1999), Regional trends in Nimbus-7 OLR: Effects of a spectrally nonuniform albedo, *J. Clim.*, *12*, 1458–1466, doi:10.1175/1520-0442(1999)012<1458:RTINOE>2.0.CO;2.

Tiao, G. C., G. C. Reinsel, D. Xu, J. H. Pedrick, X. Zhu, A. J. Miller, J. J. DeLuisi, C. L. Mateer, and D. J. Wuebbles (1990), Effects of autocorrelation and temporal sampling schemes on estimates of trend and spatial

correlation, *J. Geophys. Res.*, *95*, 20,507–20,517, doi:10.1029/JD095iD12p20507.

Ungar, S. G., J. S. Pearlman, J. A. Mendenhall, and D. Reuter (2003), Overview of the Earth Observing One (EO-1) mission, *IEEE Trans. Geosci. Remote Sens.*, *41*(6), 1149–1159, doi:10.1109/TGRS.2003.815999.

von Storch, H., and F. W. Zwiers (1999), *Statistical Analysis in Climate Research*, 484 pp., Cambridge Univ. Press, New York.

Weatherhead, E. C., et al. (1998), Factors affecting the detection of trends: Statistical considerations and applications to environmental data, *J. Geophys. Res.*, *103*(D14), 17,149–17,161, doi:10.1029/98JD00995.

Wielicki, B. A., and L. Parker (1992), On the determination of cloud cover from satellite sensors: The effect of sensor spatial resolution, *J. Geophys. Res.*, *97*(D12), 12,799–12,823.

Wielicki, B. A., R. D. Cess, M. D. King, D. A. Randall, and E. F. Harrison (1995), Mission to planet Earth: Role of clouds and radiation in climate, *Bull. Am. Meteorol. Soc.*, *76*(11), 2125–2153, doi:10.1175/1520-0477(1995)076<2125:MTPERO>2.0.CO;2.

Wielicki, B. A., et al. (1996), Clouds and the Earth's Radiant Energy System (CERES): An Earth observing system experiment, *Bull. Am. Meteorol. Soc.*, *77*, 853–868, doi:10.1175/1520-0477(1996)077<0853:CATERE>2.0.CO;2.

Wielicki, B. A., et al. (2005), Changes in Earth's albedo measured by satellite, *Science*, *308*(5723), 825, doi:10.1126/science.1106484.

Young, D. F., P. Minnis, D. R. Doelling, G. G. Gibson, and T. Wong (1998), Temporal INTERPOLATION methods for the Clouds and the Earth's Radiant Energy System (CERES) experiment, *J. Appl. Meteorol.*, *37*, 572–590, doi:10.1175/1520-0450(1998)037<0572:TIMFTC>2.0.CO;2.

C. A. Algieri, Climate Sciences Department, Lawrence Berkeley National Laboratory, Berkeley, CA 94720, USA.

W. D. Collins and D. R. Feldman, Earth Sciences Division, Lawrence Berkeley National Laboratory, 1 Cyclotron Rd., MS 50A4037, Berkeley, CA 94720, USA. (drfeldman@lbl.gov)

P. A. Pilewskie, Laboratory for Atmospheric and Space Physics, University of Colorado at Boulder, Duane Physics, Rm. G135 Campus Box 311, Boulder, CO 80309-0311, USA.

Y. L. Roberts, Department of Atmospheric and Oceanic Science, University of Colorado at Boulder, UCB 392, Boulder, CO 80303, USA.